Synchronized autonomous sampling reveals coupled pulses of biomass and export of morphologically different diatoms in the Southern Ocean

Stéphane Blain, Mathieu Rembauville, Olivier Crispi, Ingrid Obernosterer

Synchronized autonomous sampling reveals coupled pulses of biomass and export of morphologically different diatoms in the Southern Ocean

Stéphane Blain*, Mathieu Rembauville, Olivier Crispi and Ingrid Obernosterer

Sorbonne Université, CNRS, Laboratoire d'océanographie microbienne, avenue Pierre Fabre, 66650 Banyuls sur mer, France

stephane.blain@obs-banyuls.fr

mathieu.rembauville@obs-banyuls.fr

olivier.crispi@obs-banyuls.fr

ingrid.obernosterer@obs-banyuls.fr

* Corresponding author

keywords : carbon stock, carbon export, diatoms, southern ocean, aggregates, seasonal time series, autonomous sampling

Running head : Pulses of diatom biomass and export

ABSTRACT.

The Southern Ocean hosts a large diversity of diatoms that play a major role in carbon fluxes. How the seasonal dynamics in the abundance of specific taxa in surface waters are linked to their contribution to carbon export remains, however, poorly understood. We present here synchronized observations from autonomous samplers deployed in the mixed layer (42 m) and at depth (300m) during an entire productive season (October 2016 to March 2017) in the iron fertilized region of the central plateau of Kerguelen. Microscopic observations of surface water collected every 11 days revealed 30 different diatom taxa, each contributing to > 1% of total carbon biomass throughout the season. The synchronised sampling revealed a common pattern for diatom taxa belonging to 12 different genera, consisting, for a given taxon, in short pulses of abundance in surface waters followed by export. We explain these coupled dynamics by the formation of aggregates that are produced when a critical diatom cell abundance is reached. This control of the maximum abundance of a given diatom drives the seasonal change in the slope of the size-class distribution of the diatom community. It further constrains the total carbon diatom biomass in a narrow range of values due to the inverse relationship between total diatom abundance and their community-weighted mean biomass. This coupling let us conclude that aggregate formation, and the export to depth, occurs throughout the season for diatoms with different morphologies.

Introduction

During the past 250 million years diatoms have evolved a large diversity of forms and life styles (Armbrust 2009). They are successful unicellular phototrophic organisms that are present in almost all aquatic environments. They are characterized by an ornamented siliceous cell wall with diverse forms that serve as morphological criteria for species classification, an approach that is today complemented by DNA sequencing (Malviya et al. 2016). From a biogeochemical perspective, diatoms play a central role in the carbon cycle (Tréguer et al. 2018). In the past they have contributed to the lowering of atmospheric CO_2 thanks to their efficiency to massively bury carbon in the sediment (Katz et al. 2005) and thereby formed large reservoirs of fossil fuels. In the contemporary ocean they contribute to 40 % of global primary production (Nelson et al. 1995) and they sustain marine food webs. The success of diatoms is attributed to several features. On the one side, genomic adaptations (Armbrust et al. 2004; Allen et al. 2011) allow diatoms to thrive in various environments. They form blooms that can result in large sinking fluxes but require substantial nutrient supply, as provided in well-mixed water columns. This occurs preferentially in regions where turbulent water columns dominate (Margalef 1978). On the other side, the siliceous armour provides an efficient protection against predators, and possibly also against parasites and pathogens (Hamm and Smetacek 2007). The dense frustule enhances cell sinking (Smetacek 1985), necessitating elaborated strategies for maintaining the cells in the euphotic zone during the growth period (Raven and Waite 2004). The Southern Ocean hosts abundant and diverse communities of diatoms. Their ecology has been extensively described thanks to expeditions in different regions of the Antarctic circumpolar current (Queguiner et al. 1997; Tremblay et al. 2002; Leblanc et al. 2005) and to observations realised in naturally iron fertilized regions (Korb et al. 2008; Salter et al. 2012;

65 Lasbleiz et al. 2016) or during artificial fertilization experiments (Gall et al. 2001; Assmy et al.
66 2013). Additional information was also gathered from investigations on the sinking en masse
67 of the giant diatoms like *Rhizosolen*ia spp. and *Thalassiothrix* spp. (Kemp et al. 2006) or of
68 empty cells of *Corethron criophylum* (now named *Corethron pennatum (Grunow) Ostenfeld*)
69 after entering the sexual stages (Crawford et al. 1997). One of the main motivation to link
70 diatom ecology and biogeochemistry lies in the critical role they play in the carbon cycle
71 (Tréguer et al. 2018). Their role as vectors of carbon export in the water column and storage
72 at the seafloor has been demonstrated using sediment traps (Salter et al. 2012; Rigual-
73 Hernández et al. 2015; Rembauville et al. 2015a) and by the examination of sediments (Allen
74 et al. 2005; Armand et al. 2008; Rigual-Hernández et al. 2016). Considering all these
75 observations, conceptual frameworks linking diatom ecology and the carbon cycle in the
76 Southern Ocean were derived.
77 Different biogeochemical roles were attributed to different diatom taxa (Quéguiner 2013;
78 Assmy et al. 2013). For example, fast growing taxa characterized by en masse sinking
79 behaviour (e.g. *Chaetoceros*, *Thalasssiosira*) were described as carbon sinkers or type 1, and
80 highly silicified slow growing species as silica sinkers or type 2. The dominance of one
81 category over the other leads to a strong decoupling between the carbon and silicon cycles
82 (Assmy et al. 2013). However, the coupling between the temporal dynamics of surface
83 stocks and export at depth of diatoms at the taxon level is still poorly studied and
84 understood, because it requires to collect samples evenly spaced in time during the entire
85 growth season. This task is particularly challenging in the open ocean and even more in
86 harsh environments like the Southern Ocean. In our study we have addressed this issue
87 using synchronized autonomous samplers deployed for 4 months both within (42 m) and
88 below (300 m) the surface mixed layer. Our samples were collected in the long lasting

89 Southern Ocean blooms that are sustained by natural iron fertilization above the Kerguelen
90 Plateau (Blain et al. 2007). Throughout the season, these blooms are dominated by a
91 succession of different diatom taxa (Lasbleiz et al. 2016; Rembauville et al. 2017). This
92 contrasts with spring to summer transitions in most oceanic regions where a succession of
93 diatoms and non diatoms are observed (Barber and Hiscock 2006). The Kerguelen plateau
94 waters therefore represent a unique environment for our investigations.
95

96 MATERIALS AND METHODS

97 **Moorings.**

98 Two moorings were deployed during the SOCLIM cruise (doi/10.17600/16003300), one for
99 the sediment traps on 13 October 2016, and one in subsurface waters on 18 October 2016.
100 Both moorings were recovered on 7 April 2017. The sub surface mooring (50°37'135 S /
101 072°06'179 E, bottom depth 527m) was equipped with an aluminium framework located at
102 42 m below the surface that contained a remote access sampler (RAS Mac Lane) allowing the
103 collection of 48 x 500 mL samples. We collected 12 samples of unfiltered seawater every 11th
104 day, preserved either with glutaraldehyde or mercury chloride, and 18 filtered and unfiltered
105 samples preserved with mercury chloride (Fig 1a). The sub surface framework was also
106 equipped with a CTD sensor (SeabirdSBE 16) and a current meter (Aquadrop). Below the
107 instrument package and down to 300 m, the mooring line was equipped with additional
108 temperature (SBE 56) and temperature/salinity sensors (SBE 37) to monitor changes in the
109 mixed layer depth. The second mooring (50°38'344 S/ 71°59'854E, bottom depth 527 m) was
110 equipped with a Technicap PPS3 sediment trap (0.125 m^2 collecting area, 4.75 aspect ratio)
111 located at 300 m below the surface. The 12 cups (250 ml) were filled with 5% formalin
112 hypersaline solution buffered at pH=8 with sodium tetraborate. The collection time for each
113 cup was 11 days. After recovery of the RAS mooring the samples were immediately
114 transferred from the bag into 500 mL clean polycarbonate bottles and stored in the dark at
115 room temperature until processing in the laboratory. For the sediment traps, 1 ml of the
116 supernatant of the cups were replaced by fresh hypersaline formalin buffered (pH=8)
117 solution before storage at room temperature. Upon recovery of the cups in the laboratory,
118 the swimmers were removed and the samples split into eight aliquots using a Jencons
119 peristaltic splitter (Rembauville et al. 2015b)

Microscopy and morphometry

Microscopic observations were conducted within four months after recovery of the moorings. For the identification of diatoms, counting and size measurements, we used the protocol described by (Salter et al. 2012) and modified by Rembauville et al. 2015a that allows to separately consider full and empty cells. This issue is critical for our work which aims to reconstruct the carbon flux and stock attributed to diatoms. For the preparations of diatom counting (RAS or TRAP) the samples were processed as follows. For the RAS, depending on the diatom abundance, 20 mL, or 2 mL diluted with 18 mL of artificial seawater (S=34), were decanted in a Sedgewick Rafter counting chamber (Pyser SGE S52, 1mL chamber volume). For the trap samples, 2mL of one-eight aliquot was diluted with 18 mL of artificial seawater and decanted in a Sedgewick Rafter counting chamber. Diatoms were enumerated and identified under an inverted microscope with phase contrast (Olympus IX170) at magnification 400X. The morphometric measurements were done using high resolution images (Olympus DP71 camera) and Fiji image processing software. The biovolume was calculated from morphometric measurements (Hillebrand et al. 1999). The carbon content was derived from biovolumes using allometric relationships reported in the literature (Menden-Deuer and Lessard 2000; Cornet-Barthau et al. 2007) and taking into account specific relationships for spores (Rembauville et al. 2015a). The size-abundance distributions of the diatom community collected at a given time point was based on an octave (log2) scale of cell volume.

Diatom carbon stocks and export fluxes.

The carbon stock accounted for by diatoms was calculated by summing up the contributions of the different taxa. The integrated diatom carbon stock was calculated by multiplying the

143 total carbon contained in full diatoms (POC_{diat}) by the mean mixed layer depth at the

144 sampling time.

145 The export flux of diatoms was calculated using the equation:

146 $$Cell\ flux = N_{diat} \times d \times 8 \times V_{aliquot} \times \frac{1}{0.125} \times \frac{1}{11} \times k$$

147 Where N_{diat} (cell m^{-2} d^{-1}) is the number of cells counted in one chamber, d is the dilution

148 factor, $V_{aliquot}$ is the volume of the aliquot, and k is the fraction of the chamber counted.

149 The diatom flux was then converted to POC flux for each taxon using allometric equations.

150 **Biogeochemical analysis**.

151 Dissolved major nutrients (NO_3^- and $Si(OH)_4$) in the RAS were measured in the 0.8 µm filtered

152 (polycarbonate filters) samples preserved with mercuric chloride using standard protocols

153 that have been previously applied to samples of this site (Blain et al. 2015).

154 **Community weighted mean (CWM)** .

155 CWM is defined using the equation

156 $$CWM = \sum_{i=1}^{N} p_i \times C_{diat,i}$$

157 where for the taxa i, p_i is its relative abundance and $C_{diat,i}$ is its carbon content.

158 To estimate the effect of the variability of the diatom composition on the CWM we

159 simulated virtual diatom communities. We first randomly selected 14 taxa among the 30

160 taxa contributing to at least 1% of the biomass and then we allocated to these selected

161 diatom taxa a random abundance ranging between 0 and their respective maximum

162 abundance observed during the season. Finally N_t and CWM were calculated. The simulation

163 was repeated 1000 times.

164 **Calculation of the critical cell concentrations**.

165 The critical cell concentration was calculated according to the equation of (Jackson 1990) .

166 $C_{Cr}(cell\ m^{-3}) = \frac{0.096 \times \mu}{\alpha \times \gamma \times ESR^3}$ where ESR is the Equivalent Spherical Radius (m), μ is the net

167 growth rate (s^{-1}) , α is the stickiness and γ is the shear rate (s^{-1}) estimated according to the

168 formulation (MacKenzie and Leggett 1993).

169 $\gamma = \sqrt{\frac{\varepsilon}{\vartheta}}$ where $\varepsilon = \left(\frac{\tau}{\rho_w}\right)^{3/2} \times \frac{1}{kZ}$

170 τ is the mean wind stress of 0.22 Nm^{-2} for the period of interest obtained from the Japanese

171 55-yr reanalysis (JRA-55; available online at http://jra.kishou.go.jp). ν is seawater kinematic

172 viscosity (10^{-6} m^2s^{-1}), ρ_w is the seawater density in the mixed layer (1027 kg m^{-3}). k is the von

173 Kármán constant (0.41) and Z is the mixed layer depth (70 m).

174 Simulations represented in SI Fig. 3 were obtained using the equations above with different

175 values of α (0.1, 0.25, 0.5 and 1) and μ (0.05 and 0.13 d^{-1}).

176

177 RESULTS

178 **Environmental context and temporal phytoplankton bloom dynamics**

179 The region of interest for our study is located south-east of Kerguelen island on the central
180 part of the Kerguelen Plateau (Figure 1a). The sampling site is located in a zone that has
181 been identified during previous studies in Jan-Feb 2005 (Blain et al. 2007) and Oct-Nov 2011
182 (Blain et al. 2015) as the core of the Kerguelen bloom. The ocean colour satellite images for
183 the season 2016-2017 confirm that the large bloom, typical of this region, was also present
184 during the time period considered here. The temporal variations of surface chlorophyll in the
185 vicinity of the sampling site show the succession of two blooms peaking in November and
186 January (Figure 1B). This seasonal pattern is consistent with the dual blooms as revealed
187 from the climatology for this site (Figure 1B). Ocean colour images combined with back-
188 trajectories derived from current speeds and directions at 42 m (SI Figure 1) show that the
189 horizontal advection of surface water parcels that reached the sampling site during a time
190 step of 11 days did not result in large variability of chlorophyll. The influence of spatial
191 variability was therefore limited and we will interpret changes observed at the sampling site
192 as mainly resulting from temporal variability.

193 The seasonal changes of the mixed layer depth (MLD) show that all the samples collected by
194 the RAS were located in the mixed layer (Figure 2A). The variation of diatom carbon biomass
195 integrated over the mixed layer, which accounted for the surface biomass (Pellichero et al.
196 2020), presented similar temporal variations to chlorophyll concentrations (Figure 2C). The
197 build-up of diatom biomass affected the concentrations of major nutrients in surface waters
198 (Figure 2D). The concentrations of nitrate and silicic acid were high at the beginning of the
199 season and decreased during the first bloom. This decrease was much larger for silicic acid

than for nitrate. Silicic acid concentrations increased slightly after the first bloom before being further depleted after the second bloom.

Temporal dynamics of surface diatom communities

Main taxa contributing to carbon biomass

Throughout the season, the Kerguelen blooms were dominated by diatoms (Lasbleiz et al. 2016; Rembauville et al. 2017), in contrast to blooms in temperate regions where diatoms are replaced by other phytoplankton during part of the productive season (Barber and Hiscock 2006). For the RAS time series, diatoms accounted for 89 ± 9 % of carbon phytoplankton biomass observed by microscopy supporting the idea of diatom dominance. Because we wanted to explore the relationship between biogeochemistry (carbon biomass and export) and composition of the diatom community, we describe the latter using microscopic observations rather than DNA sequencing. In this context, the advantages of microscopic observations are that they allow the taxonomic identification, the determination of absolute counts of full cells (i.e; containing carbon) and quantitative estimates of the carbon content (C_{diat}) derived from size measurements (Hillebrand et al. 1999; Menden-Deuer and Lessard 2000; Cornet-Barthau et al. 2007). In the following, we consider only diatoms at the genus or species level (hereafter referred to as taxa) that contribute to > 1% of the total diatom C biomass (POC_{diat}). In the mixed layer, we identified a total of 30 different taxa during the entire season (Fig. 2 b). The number of taxa was relatively constant throughout the season (min =11, max =15, median=14), whereas the composition of the community varied dramatically (Fig. 2B). The first peak of Chlorophyll and POC_{diat} (Fig. 2c) was dominated by taxa with low C_{diat}, typically *Chaetoceros (Hyalochaete)*, *Thalassiosira antarctica*, including their resting spores, and other small centric diatoms. The

second maximum of Chlorophyll a and POC_{diat} was dominated by taxa characterized by high C_{diat} (*Eucampia antarctica, Corethron inerme, Ondotella weissflogii, Thalasssiothrix antarctica*) with the exception of the pennate *Pseudo-nitzchia*, a genus commonly identified in artificially iron fertilized blooms (Marchetti et al. 2012). The iconic pennate species of the Southern Ocean *Fragilariopsis kerguelensis* had substantial contributions to POC_{diat} in our first sample (25 October). Its contribution continuously decreased as the first bloom developed, became negligible during the second bloom and started to recover in late summer.

Seasonal changes of abundance, size and carbon content.

The abundance of the main diatom taxa (30 in total) contributing to the total carbon biomass POC_{diat} varied by 3 orders of magnitude and their individual biovolumes varied by more than 3 orders of magnitude (from 112 μm^3 up to 152600 μm^3). To examine how these variations affect the total carbon biomass POC_{diat}, we characterized the diatom communities observed at 12 time points during the season in two different manners.

In the first approach, we used the diatom community size spectrum. The slope of the size spectra revealed marked changes throughout the season (Table 1 and SI Fig. 2).

At the beginning of the season, the slope was within the range [-0.8,-0.7]. By mid-December which coincided with the end of the declining phase of the first bloom, the slope increased rapidly up to values in the range [-0.2,-0.3], and these values were maintained until the last week of February. These latter slopes were less significant due to one or two outliers located in the middle of the size-class range that could indicate a bi-modal distribution rather than a linear one. At the end of February, the slope increased to a value of -0.51.

If we consider that the biovolume scales with the diatom abundance, as shown by the size spectrum, and if the individual carbon content of diatoms scales with the biovolume as supported by previous studies (Menden-Deuer and Lessard 2000; Cornet-Barthau et al. 2007), it is in principle possible to sum up the contributions of the different size classes to obtain the total carbon biomass POC_{diat} of the community. However, this approach could be biased if the contribution of diatom spores to a size class is non-negligible. Indeed, the volumetric carbon content of a spore is higher than that of a vegetative cell (Rembauville et al. 2015a).

For this reason we also characterized the diatom communities using a second approach and estimated the community weighted mean (CWM) (Fig. 3A). Obviously, the CWM and the total carbon biomass POC_{diat} are linked using the equation $POC_{diat}=N_t$ x CWM where N_t is the total abundance of diatoms of the community. CWM and N_t show clear opposite seasonal trends, increasing and decreasing, respectively, throughout the season (Fig. 3A, B). These changes provided insight to the seasonal variations of the total diatom carbon biomass.

Coupling between diatom taxa in surface waters and their export

The carbon fluxes attributed to diatoms in each cup of the sediment trap are presented in Fig. 4A. The first export event was mainly collected by cups #3, #4 and #5. The cumulated flux in these 3 cups was 3.9 mmol C m^{-2} d^{-1} and it represented 60 % of the seasonal diatom carbon flux. The second event was recorded in cups # 9 and #10 and the corresponding cumulated flux was 1.4 mmol C m^{-2} d^{-1} which accounted for 21% of the seasonal diatom carbon flux. The seasonal pattern of diatom carbon export was remarkably similar to those observed in 2011-2012 at the same site (Rembauville et al. 2015b).

The relative contributions of the different taxa to diatom carbon export are shown in Fig. 4B. The first event was entirely dominated by the export of *Chaetoceros* and *Thalassiosira* resting spores while more diverse taxa were contributing to the second event. For the latter, when cups #9 and #10 are cumulated, the relative contributions of the different taxa were: *Chaetoceros* resting spores (43%), *Pseudo-nitzschia heimii* (2%), *Pseudo-nitzschia lineola* (3%), *Navicula directa* (0.7%), *Eucampia antarctica* (20.4%), *Corethron inerme* (4.2%), *Odontella weisflogii* spores (15.3%), *Proboscia inermis* (1.3%), *Thalassiothrix antarctica* (3,6%), *Membraneis challenger* (5%), *Rhizosolenia styliformis* (1.5%), *Asteromphalus hookeri*(1.7%).

The synchronized sampling of diatom communities in the mixed layer and in the sediment traps (Fig. 2A) allowed a detailed investigation of the coupling between the dynamics of the abundance of individual diatom taxa in the mixed layer and of their export at 300 m. To compare both dynamics we calculated, for a given genus, its relative contribution at each time point to its total seasonal abundance and to its total seasonal export flux (Fig. 5).

It is evident that the maximum seasonal abundance of the different diatom genera in the mixed layer occurred during a short time period, closely followed by a carbon export event of the same genus. We observed that more than 44.2 % (for *Thalassionema*) and up to 100 % (for *Proboscia*) of the seasonal export attributable to a given genus took place during a relatively short time period, representing 17 % of the entire sampling period (132 days) (Table 2). To confirm the link between the dynamics of diatom surface abundance and export we estimated for each genus the correlation between the two time series with different time lags (SI Fig. 3). The correlation is significant for 10 of the genera, the exceptions being *Fragilariopsis* and *Odontella*. The time lag leading to the best correlation between both time series was 0 day for *Membraneis*, *Thalassiosira*, 11 days for *Proboscia*,

294 *Rhizosolenia*, *Eucampia*, *Thalassionema* and *Chaetoceros* and 22 days for *Corethron* and
295 *Thalassiothrix*.
296
297 DISCUSSION
298 Our study was designed to address the coupling between the seasonal dynamics of diverse
299 diatoms in the surface layer and their export at depth. Our major aim was to refine previous
300 conceptual views both on a temporal scale and on the taxon level, and thereby to make an
301 important step forward. Thanks to the seasonal coverage with good temporal resolution,
302 and to the synchronized observations between the surface layer and at depth we are able to
303 reveal a common pattern for diatom species belonging to 10 different genera that are short
304 pulses of surface abundance followed by export.
305 Short-term artificial iron fertilization experiments in the Southern Ocean and more
306 specifically the 35 days long EIFEX cruise (Smetacek et al. 2012) revealed the critical role of
307 the pulsed nature of POC export due to boom-and-burst diatoms (Assmy et al. 2013)
308 exemplified by *Chaetoceros dichaeta*. On a seasonal scale, the pulsed export of different
309 diatom taxa was inferred from sediment trap deployments in the Australian sector of the
310 Southern Ocean. The relative abundance of *Pseudo-nitzschia* and of the small *Fragilariopsis*
311 spp. in sediment traps was closely related to POC pulses in the Polar Front and in the Sub
312 Antarctic zones (Rigual-Hernández et al. 2016). Similar observations were made for
313 *Fragilariopsis kerguelensis* and *Thalassiothrix antarctica* in the Antarctic zone (Rigual-
314 Hernández et al. 2015). However, seasonal changes of the surface diatom communities were
315 not described in these previous studies, limiting further investigation of the origin of these
316 diatom pulses for carbon export. In addition, empty and full diatom cells were not
317 distinguished by the methodology applied (Romero et al. 2000).

318 Our work provides evidences of the pulsed export of diatoms for additional diatom
319 taxa, but it also allows us to go a step further and to address the question: what causes such
320 a common pattern? To answer this question, we start with the examination of the seasonal
321 changes of diatom abundance and size in the mixed layer. The maximum abundance reached
322 during the season by diatoms belonging to 12 different genera was strongly related to size,
323 characterized by the spherical equivalent radius (Fig 6 and SI Fig. 4).
324 Our simulation (Fig. 3D) shows that this unique constraint, that is size, produces an
325 envelope of communities characterized by CWM and N_t consistent with the communities
326 observed in situ.
327 The slopes of the size-class spectrum determined in our study at the beginning of the
328 season were close to those reported for coastal eutrophic and upwelling ecosystems
329 (around -0.8; Cermeño and Figueiras 2008), while slopes up to -1.3 are reported for
330 subtropical regions (Cermeño and Figueiras 2008). A 10 year time series at a shelf station in
331 a temperate region revealed little variation (-0.96), with only episodically low slopes (-0.6)
332 during the relaxation of upwelling (Huete-Ortega et al. 2010). In comparison, the slopes
333 obtained in the present study during the second part of the season (-0.29 to -0.25) are low.
334 Both, the changes of the slope of the size-class spectrum (Table 1) and of the CWM are
335 explained by the replacement of small and abundant diatoms during the first part of the
336 season by large and less abundant diatoms during summer.
337 The paradigm that small phytoplankton dominate when resources are limited, as is
338 typically the case in oligotrophic gyres, and that large cells thrive when sufficient amounts of
339 resources are available, typical for coastal environments or upwelling regions, has been
340 invoked to explain spatial differences in the slopes of the phytoplankton community size
341 spectrum and can be explained by the size scaling of nutrient requirements and growth

342 (Irwin et al. 2006). Our observations that large cells dominate in summer when essential
343 nutrients like silicic acid (Fig. 2D) and iron (Blain et al. 2008) are at their lowest values seems
344 at odds with this explanation. Therefore, another mechanism should control the size
345 distribution of the diatom communities in this region. We propose the formation of diatom
346 aggregates as an explanation. The first observations of diatom aggregates have been
347 reported by (Billett et al. 1983; Smetacek 1985). Theoretical approaches have shown that
348 the formation of aggregates occurs when a critical cell abundance is reached for given
349 environmental and cell properties (Jackson 1990) and such predictions have been confirmed
350 in situ (Boyd et al. 2002). The critical abundances calculated by Jackson's model were also
351 consistent with POC and biovolumes determined at the Bermuda Atlantic time series and off
352 southern California (Jackson and Kiørboe 2008). In the Kerguelen bloom the formation of
353 aggregates has been suggested to occur during the spring bloom based on in situ
354 observations of changes in the size spectrum and modelling (Jouandet et al. 2014). The
355 critical abundance depends on both, the properties of diatoms (ESR, stickiness, and net
356 growth rate) and the properties of the environment (shear rate). When applying our data to
357 an aggregation model (Jackson 1990), it showed that the observed maximum abundances
358 for individual taxa (Fig. 6), or for size classes (SI Fig. 4) was determined by the net-growth
359 rate and the stickiness of individual diatom taxa.
360
361 If we look at the results of the model considering different stickiness values, a parameter
362 that can vary largely depending on the taxa (Kiørboe et al. 1990), the agreement between the
363 model and the data is better with α=1 for small cells (μ=0.13 d^{-1}). The maximum abundances are
364 even below the critical abundances predicted by the model with this value of α. It is conceivable
365 that the ESR of small cells is underestimated in the context of the formation of aggregates

366 because it does not take into account the presence of spines, which likely increase the ESR. For
367 the larger cell (or size classes), that were growing around μ=0.05 d^{-1}, the better fitting is
368 obtained for values of α in the range 0.5-0.25 (Fig. 6 and SI Fig. 4). This suggests that the
369 stickiness of these larger cells would be lower. These results obtained at the diatom taxon
370 level extend the previous conclusion of Jackson and Kiørboe 2008 obtained for bulk POC that
371 the formation of diatom aggregates is a major factor of control for the maximum diatom
372 abundance and consequently for their export.
373 When aggregates formed in the mixed layer are exported below the mixed layer
374 depth, pulsed export events are expected. This was obviously the case considering the
375 pulsed export dynamics observed in the present study (Fig. 5). We note that a similar
376 seasonal pattern of carbon diatom export was observed in 2011-2012 at the same site
377 (Rembauville et al. 2015a) suggesting that there is little interannual variability in the shape
378 and magnitude of the carbon fluxes transported by diatoms. However, in the present study
379 the total seasonal flux of POC was roughly 10 times higher than in 2011-2012 suggesting a
380 large interannual variability in the carbon export due to faecal pellets. This observation is
381 puzzling and advocates for seasonal monitoring of the composition of zooplankton
382 community composition. Such observations were technically not feasible during the present
383 study, but the rapid ongoing technological developments of underwater video profilers
384 integrated to profiling floats (Claustre et al. 2020) or moorings provide promising
385 perspectives for the near future.
386 Our sediment trap samples were collected using cups filled with hypersaline
387 solution, and transported back to the laboratory for processing, including splitting. This
388 protocol is not as well adapted to preserve aggregates as the collection and direct
389 observation with gel traps (Ebersbach and Trull 2008). Considering the different estimates of

time lags we can also estimate the sinking velocity of aggregates. These are in the range 25 to 250 m d^{-1} and thus in good agreement with values determined in rolling tanks for aggregates formed with different Southern Ocean diatoms ([13- 260 m d^{-1}]; Laurenceau-Cornec et al. 2015).

Collectively, our observations let us conclude that the formation of diatom aggregates occurs throughout the season, and is driven by a threshold in the abundance of a given diatom taxon. This leads to pulsed temporal dynamics in the abundance of diatoms with diverse morphology and their export to depth. The control of the maximum abundance of a given diatom by the formation of aggregates drives the seasonal change in the slope of the size-class distribution of the diatom community. It also constrains the total carbon diatom biomass in a narrow range of values due to the inverse relationship between N_t and CWM.

404 References

405 Allen, A. E., C. L. Dupont, M. Oborník, and others. 2011. Evolution and metabolic significance of the
406 urea cycle in photosynthetic diatoms. Nature **473**: 203.

407 Allen, C. S., J. Pike, C. J. Pudsey, and A. Leventer. 2005. Submillennial variations in ocean conditions
408 during deglaciation based on diatom assemblages from the southwest Atlantic: diatom
409 record from the falkland through. Paleoceanography **20**: n/a-n/a.
410 doi:10.1029/2004PA001055

411 Armand, L. K., X. Crosta, B. Quéguiner, J. Mosseri, and N. Garcia. 2008. Diatoms preserved in surface
412 sediments of the northeastern Kerguelen Plateau. Deep Sea Research Part II: Topical Studies
413 in Oceanography **55**: 677.

414 Armbrust, A. V., J. A. Berges, C. Bowler, and others. 2004. The genome of th diatom Thalassiosira
415 pseudonana: ecoly, evolution and metabolism. Science **306**: 79–86.

416 Armbrust, E. V. 2009. The life of diatoms in the world's oceans. Nature **459**: 185–192.
417 doi:10.1038/nature08057

418 Assmy, P., V. Smetacek, M. Montresor, and others. 2013. Thick-shelled, grazer-protected diatoms
419 decouple ocean carbon and silicon cycles in the iron-limited Antarctic Circumpolar Current.
420 Proceedings of the National Academy of Sciences **110**: 20633–20638.
421 doi:10.1073/pnas.1309345110

422 Barber, R. T., and M. R. Hiscock. 2006. A rising tide lifts all phytoplankton: Growth response of other
423 phytoplankton taxa in diatom-dominated blooms: A RISING TIDE RAISES ALL
424 PHYTOPLANKTON. Global Biogeochem. Cycles **20**: n/a-n/a. doi:10.1029/2006GB002726

425 Billett, D. S. M., R. S. Lampitt, A. L. Rice, and R. F. C. Mantoura. 1983. Seasonal sedimentation of
426 phytoplankton to the deep-sea benthos. Nature **302**: 520–522. doi:10.1038/302520a0

427 Blain, S., J. Capparos, A. Guéneuguès, I. Obernosterer, and L. Oriol. 2015. Distributions and
428 stoichiometry of dissolved nitrogen and phosphorus in the iron-fertilized region near
429 Kerguelen (Southern Ocean). Biogeosciences **12**: 623–635. doi:10.5194/bg-12-623-2015

Blain, S., B. Quéguiner, L. Armand, and others. 2007. Effect of natural iron fertilisation on carbon sequestration in the Southern Ocean. Nature **446**: 1070–1075. doi:doi:10.1038/nature05700

Blain, S., G. Sarthou, and P. Laan. 2008. Distribution of dissolved iron during the natural iron-fertilization experiment KEOPS (Kerguelen Plateau, Southern Ocean). Deep Sea Research Part II: Topical Studies in Oceanography **55**: 594.

Boyd, P. W., G. A. Jackson, and A. M. WAite. 2002. Are mesoscale perturbation experiments in polar waters prone to physical artefacts? Evidence from algal aggregation modelling studies. Geophysical Research Letters **20**: doi: 10.1029/2001GL014210.

Cermeño, P., and F. Figueiras. 2008. Species richness and cell-size distribution: size structure of phytoplankton communities. Mar. Ecol. Prog. Ser. **357**: 79–85. doi:10.3354/meps07293

Claustre, H., K. S. Johnson, and Y. Takeshita. 2020. Observing the Global Ocean with Biogeochemical-Argo. Annu. Rev. Mar. Sci. **12**: 23–48. doi:10.1146/annurev-marine-010419-010956

Cornet-Barthau, V., L. Armand, and B. Quéguiner. 2007. Biovolume and biomass estimates of key diatoms in the Southern Ocean. Aquatic Microbial Ecology **48**: 295–308.

Crawford, R. M., F. Hinz, and T. Rynearson. 1997. Spatial and temporal distribution of assemblages of the diatom Corethron criophilum in the Polar Frontal region of the South Atlantic. Deep Sea Research Part II: Topical Studies in Oceanography **44**: 479.

Ebersbach, F., and T. Trull. 2008. Sinking particle properties from polyacrylamide gels during KEOPS: zooplankton control of carbon export in an area of persistent natural iron inputs in the Southern Ocean. Limnology and Oceanography **53**: 212–224.

Gall, M. P., R. Strzepek, M. Maldonado, and P. W. Boyd. 2001. Phytoplankton processes. Part 2: Rates of primary production and factors controlling algal growth during the Southern Ocean Iron RElease Experiment (SOIREE). Deep Sea Research Part II: Topical Studies in Oceanography **48**: 2571.

Hamm, C., and V. Smetacek. 2007. Armor: Why, When, and How, p. 311–332. *In* Evolution of Primary Producers in the Sea. Elsevier.

456 Hillebrand, H., C.-D. Dürselen, D. Kirschtel, U. Pollingher, and T. Zohary. 1999. Biovolume calculation
457 for pelagic and benthic microalgae. Journal of Phycology **35**: 403–424. doi:10.1046/j.1529-
458 8817.1999.3520403.x
459 Huete-Ortega, M., E. Maranon, M. Varela, and A. Bode. 2010. General patterns in the size scaling of
460 phytoplankton abundance in coastal waters during a 10-year time series. Journal of Plankton
461 Research **32**: 1–14. doi:10.1093/plankt/fbp104
462 Irwin, A. J., Z. V. Finkel, O. M. E. Schofield, and P. G. Falkowski. 2006. Scaling-up from nutrient
463 physiology to the size-structure of phytoplankton communities. Journal of Plankton Research
464 **28**: 459–471. doi:10.1093/plankt/fbi148
465 Jackson, G. A. 1990. A model of the formation of marine algal flocs by physical coagulation processes.
466 Deep Sea Research Part A. Oceanographic Research Papers **37**: 1197–1211.
467 doi:10.1016/0198-0149(90)90038-W
468 Jackson, G. A., and T. Kiørboe. 2008. Maximum phytoplankton concentrations in the sea. Limnol.
469 Oceanogr. **53**: 395–399. doi:10.4319/lo.2008.53.1.0395
470 Jouandet, M.-P., G. A. Jackson, F. Carlotti, M. Picheral, L. Stemmann, and S. Blain. 2014. Rapid
471 formation of large aggregates during the spring bloom of Kerguelen Island: observations and
472 model comparisons. Biogeosciences **11**: 4393–4406. doi:10.5194/bg-11-4393-2014
473 Katz, M. E., J. D. Wright, K. G. Miller, B. S. Cramer, K. Fennel, and P. G. Falkowski. 2005. Biological
474 overprint of the geological carbon cycle. Marine Geology **217**: 323–338.
475 doi:10.1016/j.margeo.2004.08.005
476 Kemp, A. E. S., R. B. Pearce, I. Grigorov, J. Rance, C. B. Lange, P. Quilty, and I. Salter. 2006. Production
477 of giant marine diatoms and their export at oceanic frontal zones: Implications for Si and C
478 flux from stratified oceans. Global Biogeochemical Cycles **20**. doi:10.1029/2006GB002698
479 Kiørboe, T., K. P. Andersen, and H. G. Dam. 1990. Coagulation efficiency and aggregate formation in
480 marine phytoplankton. Mar. Biol. **107**: 235–245. doi:10.1007/BF01319822

Korb, R., M. Whitehouse, A. Atkinson, and S. Thorpe. 2008. Magnitude and maintenance of the phytoplankton bloom at South Georgia: a naturally iron-replete environment. Mar. Ecol. Prog. Ser. **368**: 75–91. doi:10.3354/meps07525

Lasbleiz, M., K. Leblanc, L. K. Armand, U. Christaki, C. Georges, I. Obernosterer, and B. Quéguiner. 2016. Composition of diatom communities and their contribution to plankton biomass in the naturally iron-fertilized region of Kerguelen in the Southern Ocean G. King [ed.]. FEMS Microbiology Ecology **92**: fiw171. doi:10.1093/femsec/fiw171

Laurenceau-Cornec, E., T. Trull, D. Davies, C. De La Rocha, and S. Blain. 2015. Phytoplankton morphology controls on marine snow sinking velocity. Marine Ecology Progress Series **520**: 35–56. doi:10.3354/meps11116

Leblanc, K., C. E. Hare, P. W. Boyd, and others. 2005. Fe and Zn effects on the Si cycle and diatom community structure in two contrasting high and low-silicate HNLC areas. Deep Sea Research Part I: Oceanographic Research Papers **52**: 1842–1864. doi:10.1016/j.dsr.2005.06.005

MacKenzie, B. R., and W. C. Leggett. 1993. Wind-based models for estimating the dissipation rates of turbulent energy in aquatic environments: empirical comparisons. Marine Ecology Progress Series **94**: 207–216.

Malviya, S., E. Scalco, S. Audic, and others. 2016. Insights into global diatom distribution and diversity in the world's ocean. Proceedings of the National Academy of Sciences **113**: E1516–E1525. doi:10.1073/pnas.1509523113

Marchetti, A., D. M. Schruth, C. A. Durkin, and others. 2012. Comparative metatranscriptomics identifies molecular bases for the physiological responses of phytoplankton to varying iron availability. Proceedings of the National Academy of Sciences **109**: E317–E325. doi:10.1073/pnas.1118408109

Margalef, R. 1978. Life-form of phytoplankton as survival alternatives in an unstable environment. Oceanologica Acta **1**: 493–509.

506 Menden-Deuer, S., and E. J. Lessard. 2000. Carbon to volume relationships for dinoflagellates,
507 diatoms, and other protist plankton. Limnol. Oceanogr. **45**: 569–579.
508 doi:10.4319/lo.2000.45.3.0569
509 Nelson, D. M., P. Tréguer, M. A. Brzezinski, A. Leynaert, and B. Quéguiner. 1995. Production and
510 dissolution of biogenic silica in the ocean: Revised global estimates, comparison with regional
511 data and relationship to biogenic sedimentation. Global Biogeochem. Cycles **9**: 359–372.
512 doi:10.1029/95GB01070
513 Pellichero, V., J. Boutin, H. Claustre, L. Merlivat, J. Sallée, and S. Blain. 2020. Relaxation of Wind Stress
514 Drives the Abrupt Onset of Biological Carbon Uptake in the Kerguelen Bloom: A Multisensor
515 Approach. Geophys. Res. Lett. **47**. doi:10.1029/2019GL085992
516 Quéguiner, B. 2013. Iron fertilization and the structure of planktonic communities in high nutrient
517 regions of the Southern Ocean. Deep Sea Research Part II: Topical Studies in Oceanography
518 **90**: 43–54. doi:10.1016/j.dsr2.2012.07.024
519 Queguiner, B., P. Treguer, I. Peeken, and R. Scharek. 1997. Biogeochemical dynamics and the silicon
520 cycle in the Atlantic sector of the Southern Ocean during austral spring 1992. Deep Sea
521 Research Part II: Topical Studies in Oceanography **44**: 69.
522 Raven, J. A., and A. M. Waite. 2004. The evolution of silicification in diatoms: inescapable sinking and
523 sinking as escape? New Phytol **162**: 45–61. doi:10.1111/j.1469-8137.2004.01022.x
524 Rembauville, M., S. Blain, L. Armand, B. Quéguiner, and I. Salter. 2015a. Export fluxes in a naturally
525 iron-fertilized area of the Southern Ocean – Part 2: Importance of diatom resting spores and
526 faecal pellets for export. Biogeosciences **12**: 3171–3195. doi:10.5194/bg-12-3171-2015
527 Rembauville, M., N. Briggs, M. Ardyna, and others. 2017. Plankton Assemblage Estimated with BGC-
528 Argo Floats in the Southern Ocean: Implications for Seasonal Successions and Particle Export:
529 Journal of Geophysical Research: Oceans **122**: 8278–8292. doi:10.1002/2017JC013067
530 Rembauville, M., I. Salter, N. Leblond, A. Gueneugues, and S. Blain. 2015b. Export fluxes in a naturally
531 iron-fertilized area of the Southern Ocean – Part 1: Seasonal dynamics of particulate organic

carbon export from a moored sediment trap. Biogeosciences **12**: 3153–3170. doi:10.5194/bg-12-3153-2015

Rigual-Hernández, A. S., T. W. Trull, S. G. Bray, and L. K. Armand. 2016. The fate of diatom valves in the Subantarctic and Polar Frontal Zones of the Southern Ocean: Sediment trap versus surface sediment assemblages. Palaeogeography, Palaeoclimatology, Palaeoecology **457**: 129–143. doi:10.1016/j.palaeo.2016.06.004

Rigual-Hernández, A. S., T. W. Trull, S. G. Bray, I. Closset, and L. K. Armand. 2015. Seasonal dynamics in diatom and particulate export fluxes to the deep sea in the Australian sector of the southern Antarctic Zone. Journal of Marine Systems **142**: 62–74. doi:10.1016/j.jmarsys.2014.10.002

Romero, O. E., G. Fischer, C. B. Lange, and G. Wefer. 2000. Siliceous phytoplankton of the western equatorial Atlantic: sediment traps and surface sediments. Deep Sea Research Part II: Topical Studies in Oceanography **47**: 1939–1959. doi:10.1016/S0967-0645(00)00012-6

Salter, I., A. E. S. Kemp, C. M. Moore, R. S. Lampitt, G. A. Wolff, and J. Holtvoeth. 2012. Diatom resting spore ecology drives enhanced carbon export from a naturally iron-fertilized bloom in the Southern Ocean. Global Biogeochemical Cycles **26**. doi:10.1029/2010GB003977

Smetacek, V., C. Klaas, V. H. Strass, and others. 2012. Deep carbon export from a Southern Ocean iron-fertilized diatom bloom. Nature **487**: 313–319. doi:10.1038/nature11229

Smetacek, V. S. 1985. Role of sinking in diatom life-history cycles: ecological, evolutionary and geological significance. Marine Biology **84**: 239–251. doi:10.1007/BF00392493

Tréguer, P., C. Bowler, B. Moriceau, and others. 2018. Influence of diatom diversity on the ocean biological carbon pump. Nature Geoscience **11**: 27–37. doi:10.1038/s41561-017-0028-x

Tremblay, J. E., M. I. Lucas, G. Kattner, R. Pollard, V. H. Strass, U. Bathmann, and A. Bracher. 2002. Significance of the Polar Frontal Zone for large-sized diatoms and new production during summer in the Atlantic sector of the Southern Ocean. Deep Sea Research Part II: Topical Studies in Oceanography **49**: 3793.

Table 1 : Seasonal changes of diatom communities size class spectrum parameters where biovolume were in μm^3 and abundance in cell L^{-1}

date	sample	slope	intercept	R_squared	p
10/25/2016	1	-0.81	7.001	0.563	0.012
11/06/2016	2	-0.82	7.683	0.529	0.017
11/17/2016	3	-0.73	7.225	0.732	0.003
11/28/2016	4	-0.71	7.082	0.745	0.002
12/09/2016	5	-0.50	6.309	0.559	0.020
12/20/2016	6	-0.48	5.801	0.270	0.123
12/31/2016	7	-0.20	5.111	0.040	0.577
01/11/2017	8	-0.25	5.413	0.120	0.360
01/22/2017	9	-0.25	5.214	0.175	0.262
02/02/2017	10	-0.22	5.067	0.361	0.115
02/13/2017	11	-0.19	4.577	0.102	0.400
02/24/2017	12	-0.51	5.731	0.400	0.090

562 **Table 2 : Diatom taxa, and biological and environmental parameters**

Diatoms	%[a]	Morphology[b]	Spores	μ[c] d^{-1}	T max[d]	$Si(OH_4)$[e] μM	NO_3[e] μM
Proboscia inermis	100	CR	N		7	3.18	22.1
Membraneis challengeri	84.3	PRap	N		10	2.45	22.8
Thalassiosira antarctica	78.7	CR	Y	0.17	2	17.9	25.4
Thalassiothrix antarctica	77.2	PArap	N		7	3.18	22.1
Rhizosolenia chunii	76.6	CR	N		7	3.18	22.1
Pseudo-nitzschia spp.	68.1	PRap	N	0.067	7	3.18	22.1
Eucampia antarctica	67.1	CMP	Y	0.072	7	3.18	22.1
Corethron inerme	65.3	CR	N	0.046	7	3.18	22.1
Odontella weisflogii	63.4	CMP	Y		7	3.18	22.1
Chaetoceros (Hyalochaete)	59.6	CMP	Y	0.13	2	17.9	25.4
Navicula directa	58.4	PRap	N		8	4.52	21.9
Fragilariopsis kerguelensis	49.6	PRap	N	0.077	2	17.9	22.8
Thalassionema nitzschioides	44.2	PRap	N	0.11	2	17.9	22.8

563

564 [a] percentage of the seasonal export achieved during the periods denoted with stars in Figure
565 3
566 [b] CR centric radial, PRap Pennate raphid, CMP centric multipolar
567 [c] net growth rate determined from the increase in cell abundance during the growing phase
568 of the population.
569 Spores: indicates whether diatom species produces spores (Y) or not (N)
570 [d] sample number when the abundance was maximum.
571 [e] Concentrations in μmol L^{-1}
572

573

574

List of figure legends:

Figure 1: Chlorophyll seasonal changes and location of the mooring site. (A) Global view of the mooring site on the central Kerguelen plateau. The white dot denotes the position of the RAS mooring overlaying monthly chlorophyll for November 2016. The white rectangle denotes the zone that is detailed in the SI Figure 1. (B) The green line presents the climatology (1998-2017) at the mooring site with standard deviation represented with the light green shaded area. The blue line represents the chlorophyll concentrations from 8-days color satellite images at the same site for the period extending from Oct 2016 to April 2017. The vertical dotted line denotes the sampling dates.

Figure 2: Seasonal changes in the Kerguelen bloom. (A) The synchronized sampling strategy was based on an autonomous sampler collecting water in the mixed layer at 42 m and a sediment trap deployed at 300 m collecting the sinking flux. The stars denote dates when phytoplankton samples were collected. The white rectangles along the x axis, numbered 1 to 12, are the periods of collection in the sediment trap cup. (B) Relative contribution of the different diatoms to the total diatom carbon biomass (POC_{diat}) at 42 m. Diatoms are ordered according to their carbon content (SI 5 Data). Abbreviations for genus names are *Asteromphalus (A.), Corethron (C.), Chaetoceros (Ch.), Eucampia (E.), Fragilariopsis (F.), Guinardia (G.), Membraneis (M.), Navicula (N.), Odontella (O.), Proboscia (P.), Pseudo-nitzschia (P.*), Rhizosolenia (R.), Thalassiothrix (T.*), Thalassiosira (T.), Thalassionema (T.#).* (C) integrated POC_{diat} in the mixed layer (black bars). The white circles denote the surface chlorophyll concentrations derived from 8 day composite images. (D) Silicic acid (white circle) and nitrate (grey square) concentrations measured in the filtered samples collected with RAS at 42 m.

Figure 3: Seasonal changes of diatom abundance in relation to carbon biomass. (A) Community Weighted Mean (B) total abundance (C) total carbon biomass. For all the plots the dots denote the value estimated from observation and the boxplot (median, first and third quartile) visualize the variability of the estimates based on 1000 simulations of diatom community assuming a normal distribution of the traits around the observed value with a variation coefficient of 0.5. (D) Diatom abundance (N_t) versus CWM for 1000 communities resulting from random composition and abundance of the different species according to observations (see methods for details). The black line represent the fitting of the equation $N_t=POC_{diat}/CWM$ with $POC_{diat}=0.097$ mg L^{-1}.

Figure 4 : Carbon export fluxes by diatoms. A) Total diatom carbon flux in each cup B) relative contribution of different taxa to total diatom carbon flux in each cup. Abbreviations for genus names are *Asteromphalus* (*A.*), *Corethron* (*C.*), *Eucampia* (*E.*), *Fragilariopsis* (*F.*), *Membraneis* (*M.*), *Navicula* (*N.*), *Odontella* (*O.*), *Proboscia* (*P.*), *Pseudo-nitzschia* (*P.**), *Rhizosolenia* (*R.*), *Thalassiothrix* (*T.**), *Thalassiosira* (*T.*), *Thalassionema* (*T.#*).

Figure 5 : Temporal changes in the relative contribution to the cumulated seasonal abundance of a given taxon (upper panels), and to the carbon export flux of the same taxon (lower panels). Vegetative cells are shown in black and spores are presented in gray. For clarity, only 1 tick every 2 cups is presented and only cup numbers 2, 6 and 10 are labeled.

Figure 6 : Comparison of the maximum seasonal abundances of the different diatom taxa (white circles), with the critical abundance derived from the aggregation model of Jackson. The shaded areas represent all the possible critical abundances considering different combinations of μ and α as indicated on the right y-axis.

ACKNOWLEDGMENT

We thank the captains and the crew of the R/V M*arion Dufresne* for their support during the cruises. We thank E. de Saint Léger, F. Pérault and L. Scoarnec from DT-INSU, and people of IPEV (Institut Polaire Paul Emile Victor) for the technical support during preparation, deployment and recovery of moorings. We also thanks Tom Trull who inspired the use of RAS for our project and Diana Davis for her valuable advises in the preparation of this equipment. We thanks the associate editor S. Menden-Deuer and the 4 anonymous reviewers for their constructive comments. This work is part of the project SOCLIM supported by the Climate Initiative of the foundation BNP Paribas, the French research program LEFE-CYBER of INSU-CNRS, IPEV, Sorbonne Université, and the Flotte Océanographique Française. The authors declare no conflict of interest.

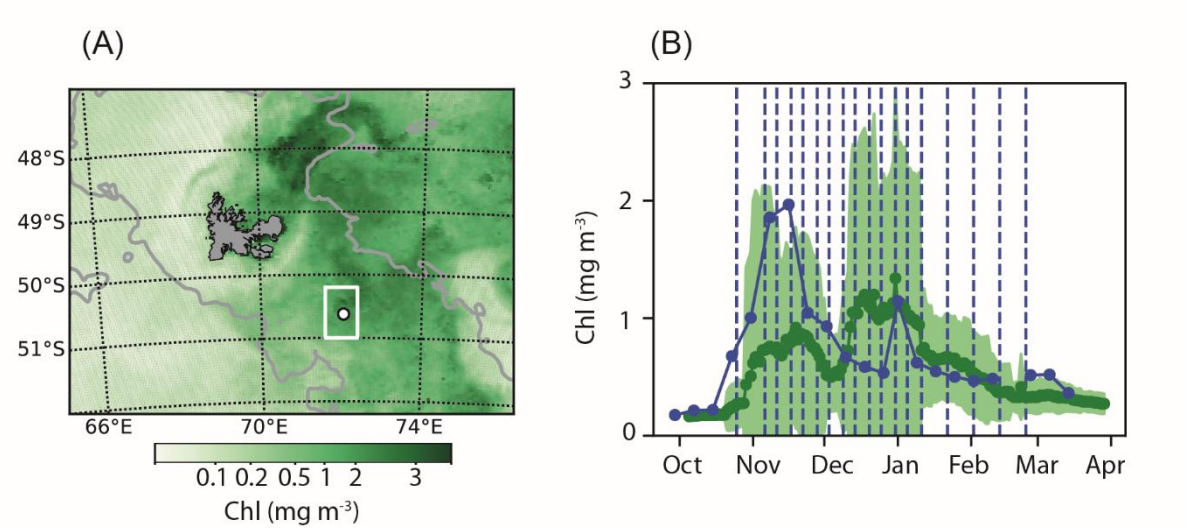
(A)
48°S
49°S
50°S
51°S
66°E
70°E
74°E
0.1 0.2 0.5 1 2 3
Chl (mg m-3)
(B)
Chl (mg m-3)
3
2
1
0
Oct
Nov
Dec
Jan
Feb
Mar
Apr

Figure 1

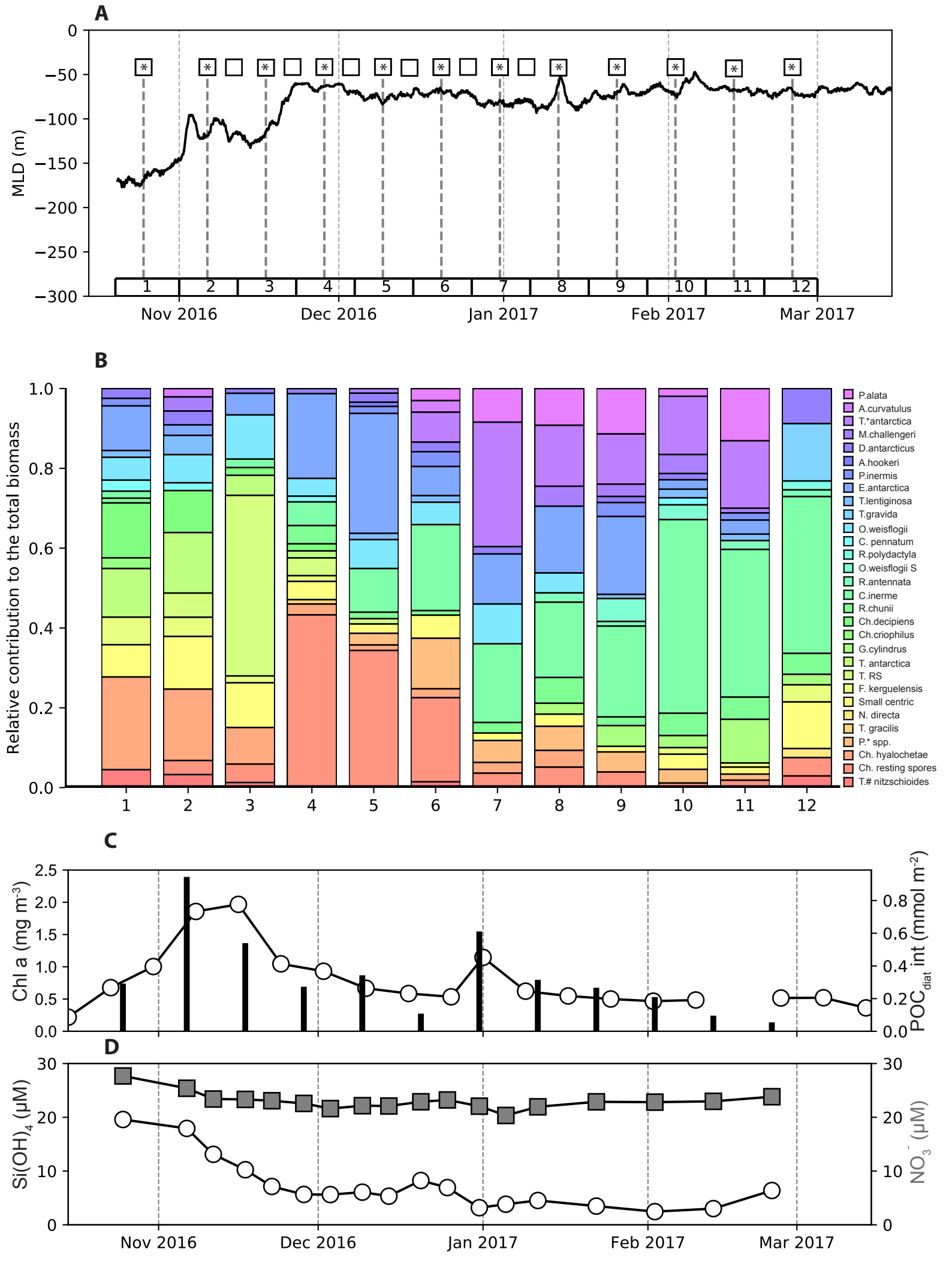
A
MLD (m)
0
−50
−100
−150
−200
−250
−300
1
2
3
4
5
6
7
8
9
10
11
12
Nov 2016
Dec 2016
Jan 2017
Feb 2017
Mar 2017
B
Relative contribution to the total biomass
1.0
0.8
0.6
0.4
0.2
0.0
P.alata
A.curvatulus
T.*antarctica
M.challengeri
D.antarcticus
A.hookeri
P.inermis
E.antarctica
T.lentiginosa
T.gravida
O.weisflogii
C. pennatum
R.polydactyla
O.weisflogii S
R.antennata
C.inerme
R.chunii
Ch.decipiens
Ch.criophilus
G.cylindrus
T. antarctica
T. RS
F. kerguelensis
Small centric
N. directa
T. gracilis
P.* spp.
Ch. hyalochetae
Ch. resting spores
T.# nitzschioides
C
Chl a (mg m-3)
2.5
2.0
1.5
1.0
0.5
0.0
POCdiat int (mmol m-2)
0.8
0.6
0.4
0.2
0.0
D
Si(OH)4 (µM)
30
20
10
0
NO3- (µM)
30
20
10
0
Nov 2016
Dec 2016
Jan 2017
Feb 2017
Mar 2017

Figure 2

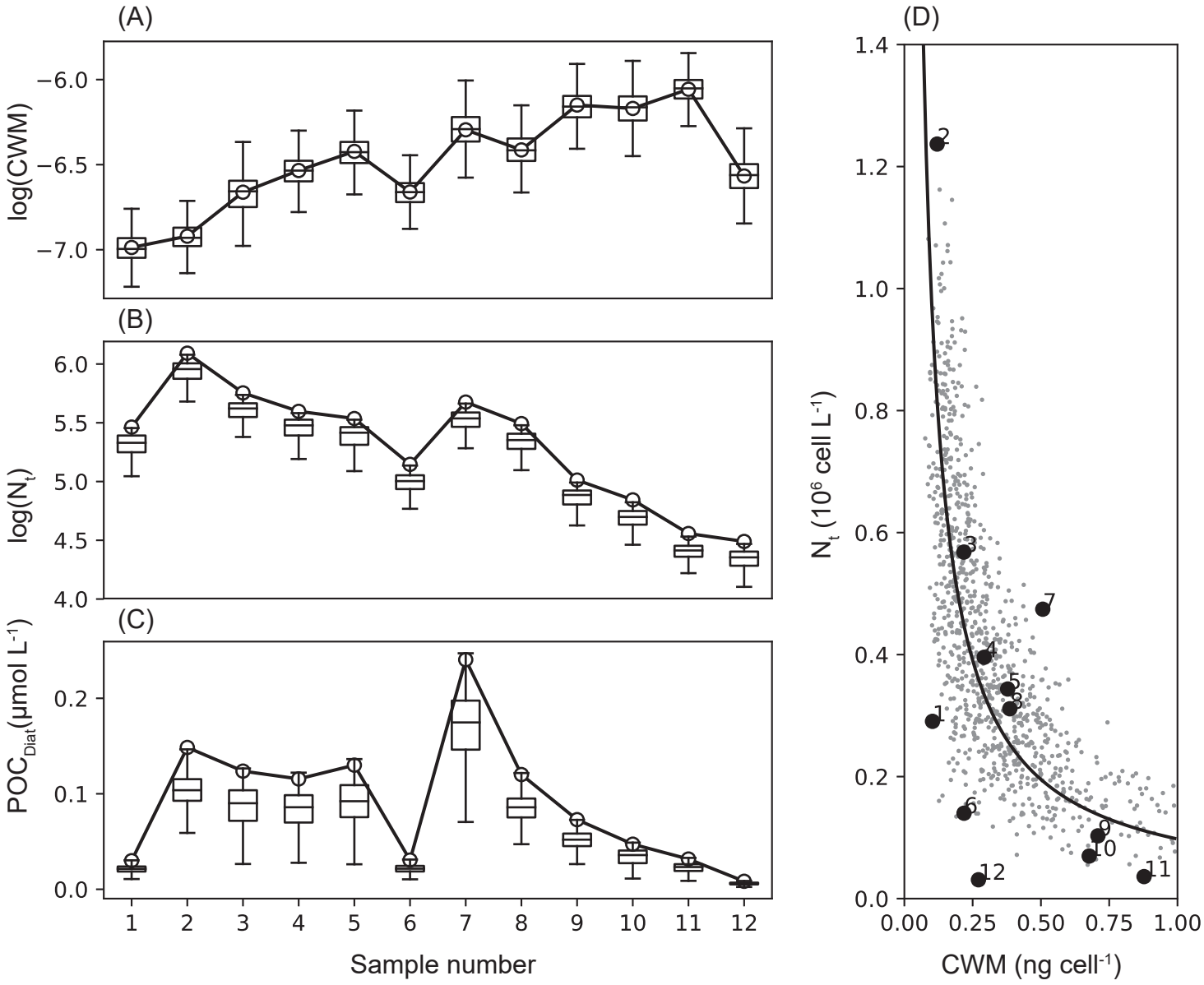
(A)
log(CWM)
−6.0
−6.5
−7.0
(B)
log(N$_t$)
6.0
5.5
5.0
4.5
4.0
(C)
POC$_{Diat}$(µmol L^{-1})
0.2
0.1
0.0
1 2 3 4 5 6 7 8 9 10 11 12
Sample number
(D)
N$_t$ (10^6 cell L^{-1})
1.4
1.2
1.0
0.8
0.6
0.4
0.2
0.0
0.00 0.25 0.50 0.75 1.00
CWM (ng cell^{-1})
1
2
3
4
5
6
7
8
9
10
11
12

Figure 3

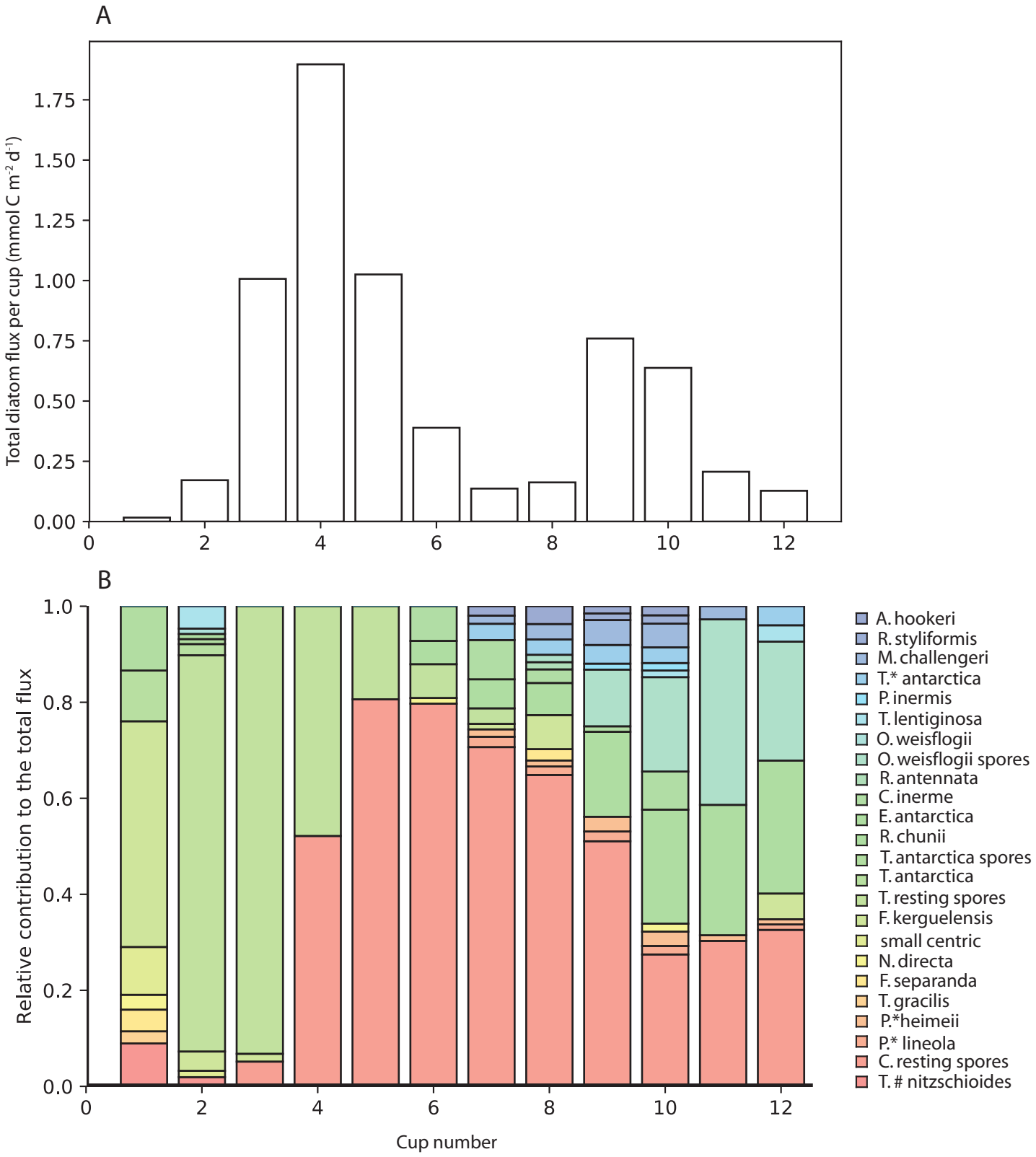
A
Total diatom flux per cup (mmol C m-2 d-1)
0.00
0.25
0.50
0.75
1.00
1.25
1.50
1.75
0
2
4
6
8
10
12
B
Relative contribution to the total flux
0.0
0.2
0.4
0.6
0.8
1.0
Cup number
A. hookeri
R. styliformis
M. challengeri
T.* antarctica
P. inermis
T. lentiginosa
O. weisflogii
O. weisflogii spores
R. antennata
C. inerme
E. antarctica
R. chunii
T. antarctica spores
T. antarctica
T. resting spores
F. kerguelensis
small centric
N. directa
F. separanda
T. gracilis
P.*heimeii
P.* lineola
C. resting spores
T. # nitzschioides

Figure 4

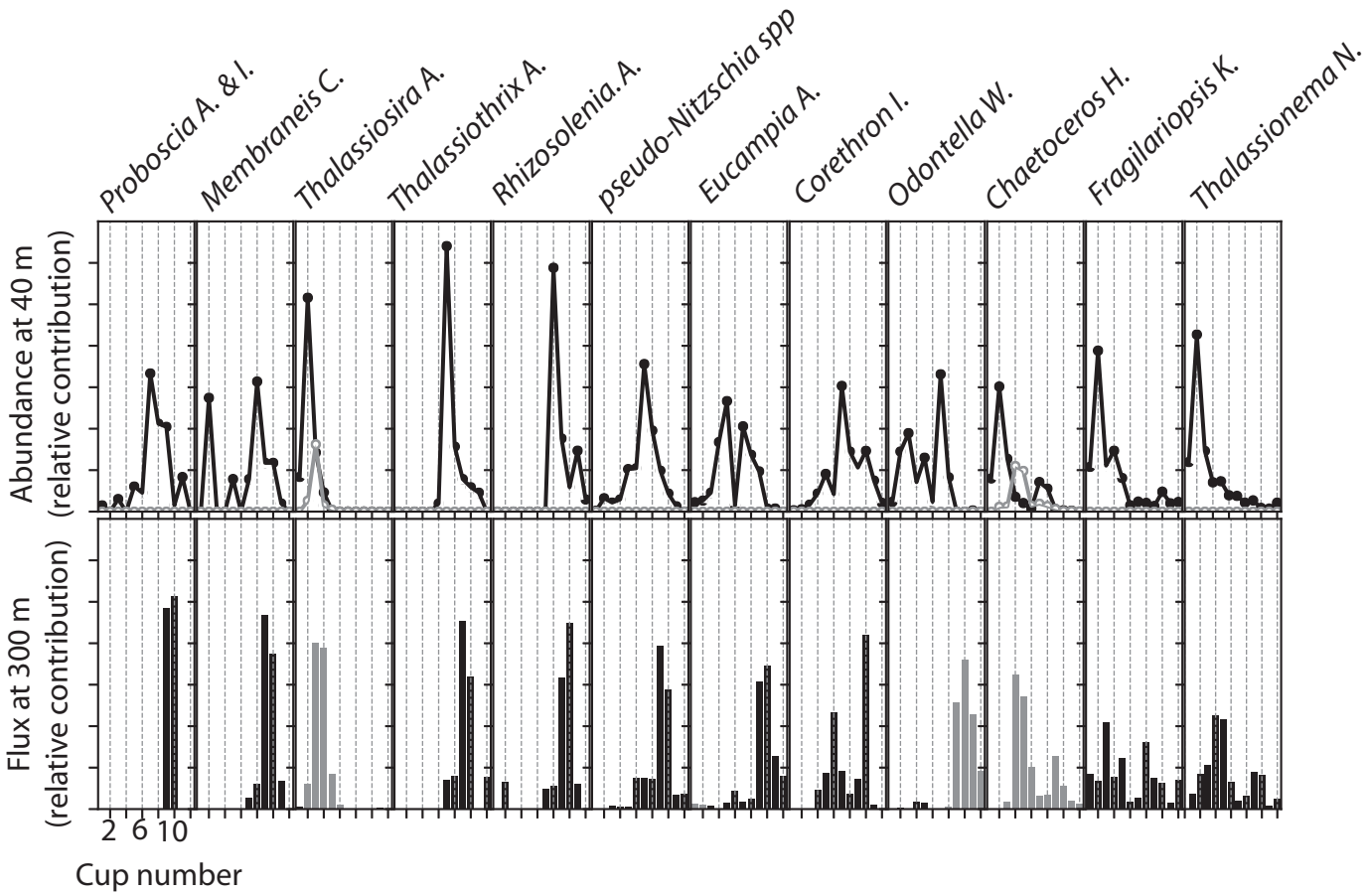
Proboscia A. & I.
Membraneis C.
Thalassiosira A.
Thalassiothrix A.
Rhizosolenia. A.
pseudo-Nitzschia spp
Eucampia A.
Corethron I.
Odontella W.
Chaetoceros H.
Fragilariopsis K.
Thalassionema N.
Abundance at 40 m
(relative contribution)
Flux at 300 m
(relative contribution)
2 6 10
Cup number

Figure 5

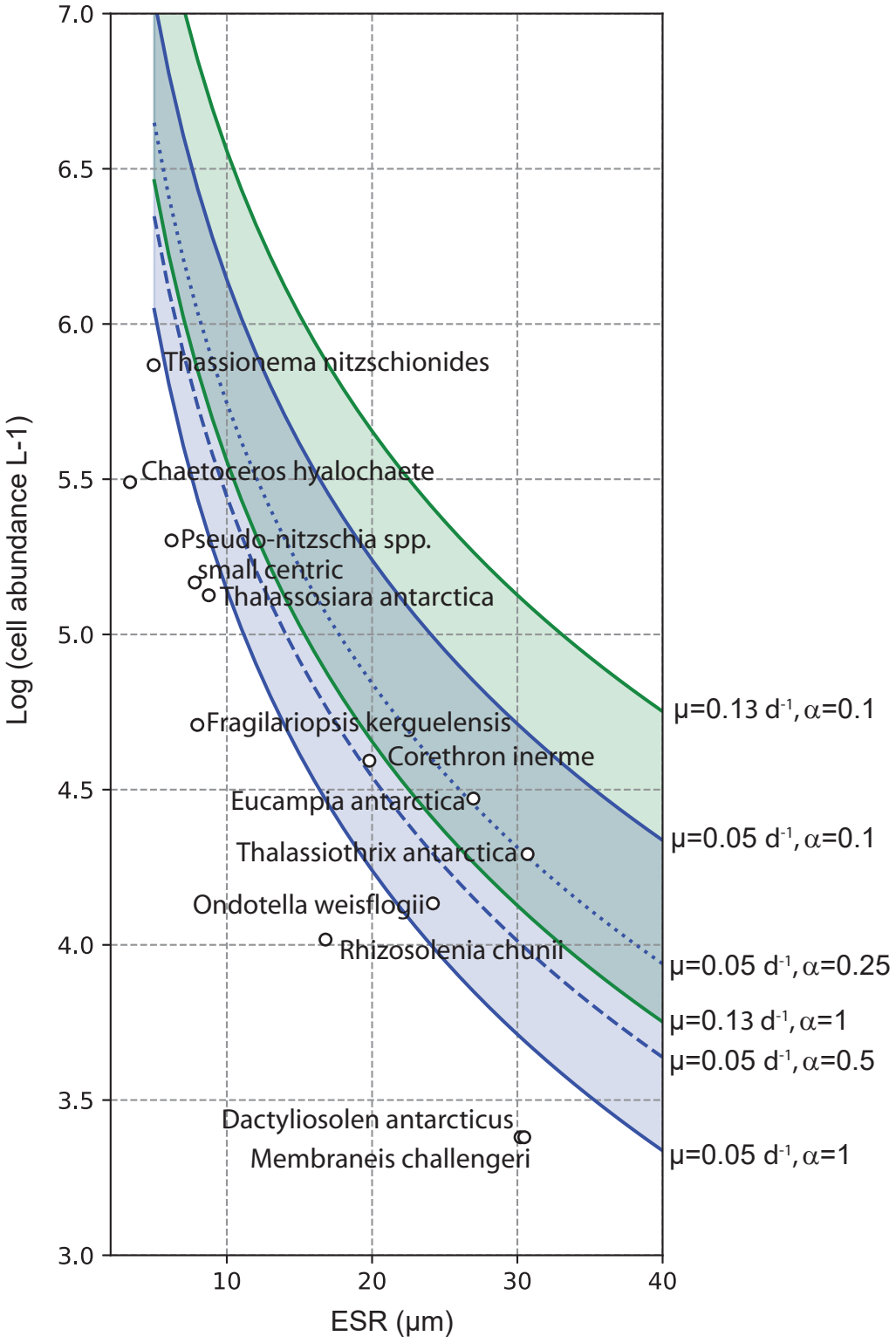
Log (cell abundance L-1)
ESR (µm)
7.0
6.5
6.0
5.5
5.0
4.5
4.0
3.5
3.0
10
20
30
40
Thassionema nitzschionides
Chaetoceros hyalochaete
Pseudo-nitzschia spp.
small centric
Thalassosiara antarctica
Fragilariopsis kerguelensis
Corethron inerme
Eucampia antarctica
Thalassiothrix antarctica
Ondotella weisflogii
Rhizosolenia chunii
Dactyliosolen antarcticus
Membraneis challengeri
µ=0.13 d-1, α=0.1
µ=0.05 d-1, α=0.1
µ=0.05 d-1, α=0.25
µ=0.13 d-1, α=1
µ=0.05 d-1, α=0.5
µ=0.05 d-1, α=1

Figure 6